Combined effect of electron and lattice temperatures on the long intersubband relaxation times of Ge/Si$_x$Ge$_{1-x}$ quantum wells

Michele Virgilio,[1,2,*] Michele Ortolani,[3,4] Martin Teich,[5,6] Stephan Winnerl,[5] Manfred Helm,[5,6] Diego Sabbagh,[7] Giovanni Capellini,[7,8] and Monica De Seta[7]

[1]*Dipartimento di Fisica "E. Fermi", Università di Pisa, Largo Pontecorvo 3, 56127, Pisa, Italy*
[2]*NEST, Istituto Nanoscienze-CNR, Piazza San Silvestro 12, 56127 Pisa, Italy*
[3]*Dipartimento di Fisica, Università di Roma "La Sapienza", Piazzale A. Moro 2, 00185 Rome, Italy*
[4]*CNR—Istituto di Fotonica e Nanotecnologie, Via Cineto Romano 42, 00156 Rome, Italy*
[5]*Institute of Ion Beam Physics and Materials Research "Helmholtz-Zentrum Dresden-Rossendorf", 01314 Dresden, Germany*
[6]*Technische Universität Dresden, 01062 Dresden, Germany*
[7]*Dipartimento di Scienze, Università di Roma Tre, Viale Marconi 446, 00146 Rome, Italy*
[8]*IHP, Im Technologiepark 25, 15236 Frankfurt (Oder), Germany*

(Received 19 September 2013; revised manuscript received 13 November 2013; published 27 January 2014)

In this paper, we have experimentally and numerically studied the nonradiative intersubband (ISB) relaxation in n-type Ge/SiGe quantum well (QW) systems. Relaxation times have been probed by means of pump-probe experiments. An energy balance model has been used to interpret the experimental differential transmission spectra and to assess the relevance in the nonradiative relaxation dynamics of both electron and lattice temperature as well as of the carrier density. The comparison between experimental data and theoretical simulation allowed us to calibrate the interaction parameters which describe the electron-optical phonon scattering in two-dimensional (2D) Ge systems. Characteristic relaxation times has been calculated and compared with those of GaAs QWs as a function of the 2D electron density, of the subband energy separation, and of the lattice and electronic temperature. We found that ISB relaxation times for the Ge/SiGe systems are generally shorter than that previously calculated when the electron distribution was neglected. Nonetheless, our main result is that the relaxation time in Ge/SiGe QW systems is longer than 10 ps, also for transition energies above the Ge optical phonon energy, up to 300 K. Furthermore, we obtained that the relaxation times are at least one order of magnitude longer than in GaAs-based systems.

DOI: 10.1103/PhysRevB.89.045311 PACS number(s): 78.67.De, 73.50.Gr

I. INTRODUCTION

Two-dimensional electron gases (2DEG) formed in silicon-germanium multiquantum wells (MQW) have recently attracted considerable attention for a number of photonic applications, such as quantum cascade lasers, emitters, modulators, and detectors [1–6], and also for energy harvesting devices based on thermoelectric [7] or photovoltaic effect [8]. The operation of these innovative unipolar devices exploits the transitions occurring between quantized states formed in the conduction or valence band of heterostructures, the subbands (SB).

In view of possible applications, Ge/SiGe heterostructures have the practical advantage that can be grown directly on Si (001) substrates by using strain-balanced heteroepitaxy and thus are compatible with the mainstream Si-based microelectronic technology. In particular, n-type Ge/SiGe MQWs, with SBs confined in the conduction band, are particularly attractive owing their low values of confinement and tunneling effective mass, comparable to those of III-V systems. Qualitative differences due to the nonpolar nature of group-IV semiconductor lattices and to the presence of degenerate anisotropic valley minima at the L point in the conduction band offer the opportunity for entirely new heterostructure design concepts. The modeling of the electronic properties of these systems requires, though, a nontrivial extension of the intersubband (ISB) transition theory, which was initially developed to describe polar III-V heterostructures with a single isotropic conduction-band minimum located at the Γ point [9–11]. The main peculiarity of the Ge/SiGe system is that the electron-phonon scattering, responsible for the nonradiative relaxation of electrons from the first-excited to the fundamental subband ($|1\rangle \rightarrow |0\rangle$), takes place only via the deformation potential coupling and not also through the long-range dipole Fröhlich interaction, as it happens in III-V polar structures [12,13]. As a consequence, relatively long intersubband relaxation times of the order of tens of picoseconds, which are beneficial for the achievement of population inversion, have been predicted up to room temperature, making n-type Ge/SiGe heterostructures very attractive for designing ISB unipolar lasers [14–18]. However, these predictions are based on empty-band calculations, thus neglecting the effect of the 2DEG distribution in the subbands, which defines the actual population of the upper and lower "states" of the optical transition. Indeed, relying on Raman and microphotoluminescence measurements, it has been demonstrated [19] that, in III-V based ISB-based photonic devices, the electrons do populate different subbands following a thermal distribution characterized by an electron temperature T_e higher than the local lattice temperature T_L. Moreover, it has been clearly shown by time-resolved ISB spectroscopy that, for high enough T_e, the relaxation time of 2DEG in excited SBs is much shorter than that expected by empty-band calculation of the electron-phonon scattering rate, especially for subband separation lower or equal to the optical phonon energy [11]. This is attributed to the thermal activation of nonradiative $|1\rangle \rightarrow |0\rangle$ ISB transitions via optical phonon

*virgilio@df.unipi.it

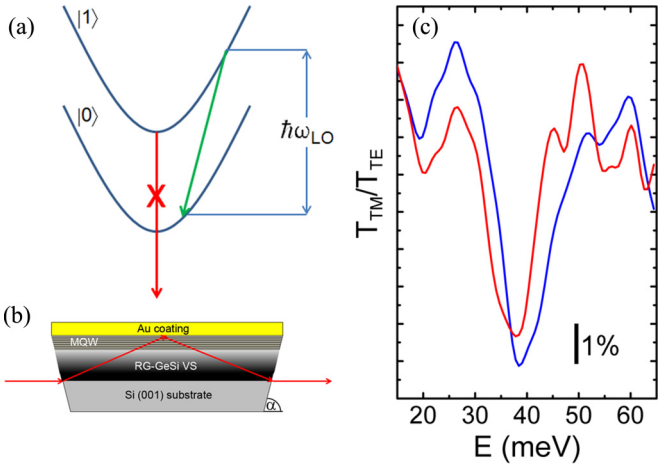

FIG. 1. (Color online) Intersubband spectroscopy of Ge/SiGe multiple quantum wells. (a) Allowed (green arrow) and forbidden (red arrow) nonradiative $|1\rangle \rightarrow |0\rangle$ electronic transition processes via optical phonon emission for subband energy separation below $h\omega_{LO}$. (b) Sketch of the single-pass waveguide configuration used in the steady-state absorption and pump-probe measurements. In the sketch, α is equal to 70°. (c) Linear dichroic transmission spectra of the S1 (red curve) and S2 (blue curve) samples, measured by FT-IR spectroscopy at $T_L = 7$ K.

emission, which involves electrons in the initial $|1\rangle$ subband, whose energy is high enough to guarantee energy conservation [see Fig. 1(a)]. In fact, scattering rates due to the interaction with optical phonons are much higher than those related to emission/absorption of acoustic phonons. Similar effects are expected to play an important role in limiting the relaxation time also in group IV semiconductor devices. Nevertheless, the effect of electron temperature on ISB relaxation times in Ge/SiGe systems was only theoretically discussed in Ref. [18], where it was recognized to be more important than in III-V compounds and crucial to obtain laser gain.

In this paper, we report terahertz pump-probe time-resolved spectroscopy, performed using the free electron laser (FEL) at the FELBE facility in Dresden, on $Ge/Si_{0.17}Ge_{0.83}$ multi-quantum wells (MQWs) [20] featuring a $|0\rangle \rightarrow |1\rangle$ absorption resonance energy $E_{10}^{abs} \sim 9$ THz (37 meV). Similar to that previously done for GaAs-based QWs [11,21], here, we exploit an energy-balance model to interpret the experimental data and to assess the relevance of both electron and lattice temperature as well as of the carrier density in the nonradiative relaxation dynamics [22]. The characteristics of the investigated samples and the experimental techniques are described in Sec. II; theoretical modeling, pump-probe results, and numerical predictions of relaxation times are reported and discussed in Sec. III; Sec. IV contains our conclusions.

II. EXPERIMENTAL

Two *n*-type Ge MQW samples (S1 and S2) featuring 12-nm-thick compressively strained Ge wells enclosed between 25-nm-thick $Si_{0.17}Ge_{0.83}$ barriers were grown by ultra-high vacuum chemical vapor deposition on a reverse-graded, partially relaxed $Si_{0.17}Ge_{0.83}$ virtual substrate deposited on a Si(001) substrate [23]. At this well width value, the absorption energy E_{10}^{abs} is close to the Ge optical phonon energy $h\omega_{LO} = 37$ meV. In sample S1 (S2), the barrier (well) region was uniformly doped by means of phosphine codeposition. In order to increase the optical absorption path, the QW structure was repeated 15 (20) times.

To perform the absorption measurements, the samples were cut in a single-pass trapezoidal prism waveguide with the lateral facets oriented at 70° with respect to the (001) direction, the MQWs being located close to the long side of the trapezium [top facet, see Fig. 1(b)]. The top facet was then coated with a Ti/Au metallization layer to further enhance the electric field component along the growth direction when transverse-magnetic (TM) polarized incident radiation is used [9]. Continuous-wave Fourier-transform infrared (FT-IR) spectroscopy was used to measure the ISB absorption spectra. The linear-dichroic transmission spectra of the two samples are shown in Fig. 1(c) and are characterized by a single absorption dip, related to the $|0\rangle \rightarrow |1\rangle$ ISB absorption resonance [9,20,23,24]. The total absorbed energy in TM polarization in the 30–40 meV range is around 5%, [see scale in Fig. 1(c)]. Notice that, in this system, there is no direct interaction between the photon beam and the phonon degrees of freedom, due to the nonpolar nature of the Ge/SiGe lattice and of the Si substrate. This is confirmed by the absence in the transverse-electric (TE) polarization spectra of any feature in the 30–40 meV range (not shown). From the analysis of S1 and S2 spectra, we estimate an absorption energy $E_{10}^{abs} = 37$ meV (39 meV) and a 2DEG carrier density in the well $n_{2D} = 1.1 \times 10^{11}$ cm^{-2} (1.4×10^{11} cm^{-2}), respectively. The full width of the absorption resonance peak in S1 (S2) was 9 (11) meV. These values are well reproduced by our multiband $k \cdot p$ numerical calculation which, starting from the structural characteristics of the MQWs samples, returns the self-consistent band edge profiles, the confined electronic states, the 2D carrier density in the well region, and the ISB absorption spectra (see Refs. [25] and [26] for a detailed model description). The slight difference in absorption energy measured in the two samples, structurally identical, is due to the different doping strategy adopted, resulting in different 2DEG density and spatial distribution. The higher n_{2D} density in S2 induces a larger depolarization shift effect, which leads to an increase of the observed absorption energy [25]. Moreover, the band bending existing in the modulation-doped structure red-shifts the transition energy in S1. We attribute the slightly larger value of the line width observed in the sample directly doped in the well (S2) to a larger impact of the impurity scattering on the dephasing time.

Degenerate terahertz pump-probe spectroscopy was performed using the FELBE terahertz tunable pulsed free-electron laser, whose photon energy was set close to the E_{10}^{abs} absorption resonance energy region ($\lambda_{FEL} = 30.4$ μm). The pump pulse excites a fraction of the electrons from the fundamental subband $|0\rangle$ into the upper subband $|1\rangle$, thus inducing an out-of-equilibrium electronic distribution. The subsequent nonradiative ISB relaxation dynamics is studied by monitoring the transient bleaching of the ISB absorption as a function of the delay time τ of a probe pulse of identical energy. The probe beam is obtained from the main laser beam via a beam splitter and a mechanically controlled mirror delay line (experimental details can be found in Ref. [27]).

The relative transmission change is thus defined as:

$$\frac{\Delta T(\tau)}{T(\infty)} = \frac{I_{pp}(\tau) - I_{pp}(\infty)}{I_{pp}(\infty)}, \quad (1)$$

where $I_{pp}(\tau)$ is the transmitted intensity of the probe beam at delay time τ. The time interval between subsequent FEL pulses (77 ns) was long enough to ensure complete relaxation before the subsequent pump pulse. The laser pulse width was estimated from the rise time of the differential transmission spectrum to be <10 ps at the chosen FEL wavelength.

III. RESULTS AND DISCUSSION

The relaxation dynamics has been theoretically addressed relying on an energy-balance model, which allows us to evaluate the differential transmission spectra measured in pump-probe experiments [22]. In this model, the time dependence of the out-of-equilibrium 2DEG energy is evaluated calculating, as a function of the probe delay time, the inelastic interactions with the pump beam and the acoustic and optical phonon baths at an equilibrium lattice temperature T_L. Thanks to the presence of fast (subpicosecond) elastic interactions between electrons [28], at each time step, the electron gas is assumed to thermalize at a time-dependent electron temperature T_e and with a chemical potential μ, both calculated self-consistently. We have thus calculated the electronic distribution function in the two subbands $|0\rangle$ and $|1\rangle$ as a function of τ, and subsequently used it to simulate the differential transmission signal. Although this approach neglects the effects of the phonon mode confinement [29], it provides a powerful tool with a level of complexity suitable to correctly capture the physics underlying the pump-probe measurements.

At the chosen subband energy separation, the dominant relaxation channel is the interaction with optical phonons while acoustic phonons give rise to longer characteristic time, of the order of hundreds of picoseconds [11,14,15]. As stated, the electron-phonon interaction in covalent crystals is mediated only by the deformation potential and, if a dispersion-less optical phonon branch is assumed, the probability per unit of time $W_{\mathrm{if}}^{\mp}(k_i)$ for an electron in subband $i = 0,1$ and in-plane momentum k_i to be scattered in subband $f = 0,1$ by phonon absorption $(-)$ or emission $(+)$ can be calculated analytically. This is due to the electron-phonon coupling, which in SiGe does not depend on the phonon momentum, as instead happens in III-V materials where the coupling amplitude is inversely proportional to its modulus. Following Ref. [12], we have

$$W_{\mathrm{if}}^{\mp}(k_i) = \Theta\left(k_{f\pm}^2\right)\frac{n_{\mathrm{dest}} m_d \Xi_{\mathrm{OP}}^2}{2\hbar^2 \rho \omega_{\mathrm{eff}}}[N(\omega_{\mathrm{eff}}, T_L) + 1/2 \mp 1/2] \times F_{\mathrm{if}}[1 - f(E_f, k_{f\pm}, T_e, \mu)], \quad (2)$$

where the upper (lower) sign indicates absorption (emission) of a phonon, Θ is the Heaviside function, $n_{\mathrm{dest}} = 1$ ($n_{\mathrm{dest}} = 3$) is the number of destination valleys involved in intra- (inter-) valley scattering events, Ξ_{OP} and $\hbar\omega_{\mathrm{eff}}$ are the related effective deformation potential and phonon energy (see later), ρ is the Ge mass density, $N(\omega_{\mathrm{eff}}, T_L)$ is the phonon Bose distribution at the lattice temperature T_L, F_{if} is the overlap between the initial and final wave functions [22], and $f(E_f, k_{f\pm}, T_e, \mu)$ is the Fermi-Dirac distribution for electrons in subband f and in-plane momentum $k_{f\pm}$ at electron temperature T_e. The value of $k_{f\pm}$ follows from energy conservation and is given by

$$\frac{\hbar^2 k_i^2}{2m_{||}} + E_i \pm \hbar\omega_{\mathrm{eff}} = \frac{\hbar^2 k_{f\pm}^2}{2m_{||}} + E_f, \quad (3)$$

where $E_{i,f}$ are the subband energy minima, and $m_{||}$ is the in-plane effective mass.

We start from Eq. (2) to calculate the net energy loss rate of the out-of-equilibrium electronic gas, in order to obtain the time dependence of the electron temperature and chemical potential. In turns, these latter quantities are used to calculate the expected differential transmission spectra (see Ref. [22]). To this purpose, we perform an average of $W_{\mathrm{if}}^{\mp}(k_i)$ over the instantaneous electronic distribution function which describes the initial and final state occupation factors [see Eq. (4) in the following]. We point out here that transitions involving absorption/emission of optical phonons can in principle occur between conduction subbands belonging either to the same (intravalley scattering) or to a different (intervalley scattering) degenerate L valley. Accordingly, in Eq. (2) inter- and intravalley processes are treated separately, being governed by two different sets of effective deformation potentials and phonon energies whose values are still not univocally accepted in the literature. In fact, these parameters have been independently evaluated in Refs. [30] and [31], calibrating Monte Carlo simulations in bulk Ge to reproduce experimental electronic transport measurements, and a slightly different set of values have been found. Moreover, Sun *et al.* [15], upon evaluating theoretically the intersubband relaxation times for Ge MQWs, claim that the intervalley processes should be suppressed in this kind of multilayer structures. Therefore, the comparison of our simulations with the experimental differential transmission spectra gives the opportunity to restrict the uncertainty on the intersubband scattering parameters of Ge multilayer systems.

In Figs. 2(a)–2(f), we plot the experimental $\frac{\Delta T(\tau)}{T(\infty)}$ spectra obtained on S1 and S2 samples at different pump power and lattice temperature. Relative transmittance changes calculated using the deformation potentials and phonon energies given in Ref. [31] ($\hbar\omega_{\mathrm{eff}} = 37.04$ meV with $\Xi_{\mathrm{OP}} = 3.5{\cdot}10^8$ eV/cm and $\hbar\omega_{\mathrm{eff}} = 23.95$ meV with $\Xi_{\mathrm{OP}} = 5.26{\cdot}10^8$ eV/cm for the intra- and intervalley scattering channels, respectively) are also displayed [32]. Due to the impossibility of an accurate estimation of the photon density in the MQW region of the samples, numerical data have been calculated adjusting the optical pump power to reproduce the measured peak value of $\frac{\Delta T(\tau)}{T(\infty)}$. Theoretical data in Fig. 2 (black solid curves) have been calculated neglecting intervalley processes except for the dashed curve in Fig. 2(a) for which intervalley scattering events have also been considered. The good agreement of the theoretical curves with the measured differential transmission signals suggests that the impact of intervalley scattering for the intersubband nonradiative dynamics in Ge/SiGe multilayer systems is negligible, as already stated in Ref. [15]. Alternatively, the scattering parameters used to evaluated the black solid lines [with $n_{\mathrm{dest}} = 1$ in Eq. (2)] can be regarded as a super-effective set which in (001) multilayer structures accounts for the joint effect of both the inter- and intravalley channels. As a matter of fact, in MQW grown on (001)

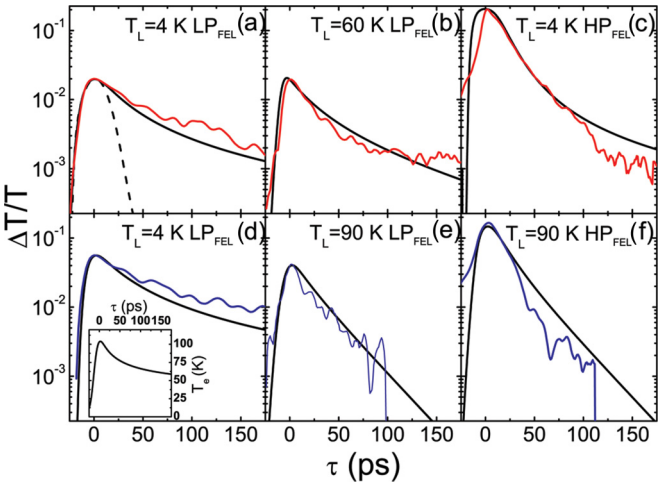

FIG. 2. (Color online) Time-resolved pump-probe signals as defined in the text, measured on samples (a)–(c) S1 and (d)–(f) S2 with laser photon energy of 40 meV at different lattice temperatures T_L and for low (LP) or high (HP) laser power density P_{FEL} (see text). Laser power values are reported in Table I. Solid black lines are the theoretical results, obtained considered only intravalley processes. The dashed curve in panel (a) represents the theoretical prediction obtained including also intervalley processes. For the experimental conditions corresponding to panel (d), the self-consistent evaluation of the electron temperature T_e is shown in the inset.

surfaces, all the L valleys are equivalent and then the distinction between inter- and intravalley processes is not mandatory.

The $\frac{\Delta T(\tau)}{T(\infty)}$ peak value increases with the amount of optical energy transferred to the 2DEG, and thus larger $\frac{\Delta T(\tau)}{T(\infty)}$ signals correspond to larger electron temperatures. At the chosen subband energy separation, higher electron temperatures correspond in turn to higher fractions of electrons in the excited subband with sufficient energy to emit optical phonons. As observed in the inset of Fig. 2(d), this emission cools down the electronic gas. As a consequence, at longer delay time, the emission of optical phonon is suppressed, and a slower relaxation rate, related to acoustic phonon emission, is observed. This process is responsible for the nonsingle exponential decay rate observed in the pump and probe experiment and well reproduced by the model (see Fig. 2).

Focusing on the S1 sample, we notice from spectra acquired at low FEL pump power [8 mW, Figs. 2(a)–2(b)], that the $\frac{\Delta T(\tau)}{T(\infty)}$ peak values are comparable. The numerical evaluation of the corresponding peak electron temperatures returns comparable values of about $T_e = 97$ and 100 K, obtained at $T_L = 4$ and 60 K, respectively. However, different initial relaxation times (57 ps at $T_L = 4$ K and 31 ps at $T_L = 60$ K) were evaluated by fitting the low delay region ($0 < \tau < 100$ ps) of the S1 $\frac{\Delta T(\tau)}{T(\infty)}$ experimental data with an exponential decay function (the corresponding theoretical values for the initial relaxation times have been extracted fitting in the same delay range the solid black curves of Figs. 2 and are reported in Table I). Being comparable to the electron temperatures, the faster initial relaxation rate observed at $T_L = 60$ K is to be entirely attributed to a larger phonon population, since a more efficient stimulated emission of optical phonons can be achieved at higher lattice temperature.

In Figs. 2(d) and 2(e), we show the $\frac{\Delta T(\tau)}{T(\infty)}$ signals obtained for S2 at low pump power (8 mW) for T_L equal to 4 and 90 K, respectively. The values for the calculated peak electron temperature and for the initial relaxation time [see inset in Fig. 2(d)] are found close to those observed in S1 at the same pump power and lattice temperature. We point out here that the pump-probe signal of S2 is higher than the one of S1, with the total energy transferred to the electron gas being $\Delta E(\mathrm{S1})/\Delta E\ (\mathrm{S2}) = 0.6$, as calculated by integration over the entire delay time domain. However, the $n_{2\mathrm{D}}$ density of electrons in S1 is calculated to be ~0.7 times smaller than in S2. As a consequence, the amount of optical energy absorbed by each electron in S1 and S2 are equal within the experimental error.

At $T_L = 4$ K, we obtain an initial relaxation time of 65 ps in conjunction with a calculated peak electron temperature of $T_e = 104$ K. As observed in S1, in the S2 sample also, upon increasing the lattice temperature, the initial relaxation time decreases, reaching a value of ~24 ps at $T_L = 90$ K.

Since in the two samples the donors are located in different regions, i.e. well and barrier, their interaction with the confined electron wave functions is different. We can thus conclude that impurity scattering does not play a major role in the nonradiative relaxation dynamics.

In Fig. 2(c), we plot the differential transmission spectrum of sample S1, measured at high power ($P_{\mathrm{FEL}} = 750$ mW). In this case, the $\frac{\Delta T(\tau)}{T(\infty)}$ peak is much larger, and the relaxation dynamic occurs at a faster timescale. The initial relaxation time is now 25 ps, i.e. more than 2 times faster than that obtained at the same lattice temperature with low pump power. Moreover,

TABLE I. Experimental (first column) and theoretical (second column) initial relaxation time, evaluated for samples S1 and S2 fitting with an exponential decay function the differential transmission spectra of Figs. 2(a)–2(f) in the first 100 ps delay range. The peak values of the differential transmission spectrum $\Delta T/T$ and of the self-consistently calculated electron temperature T_e are reported in the third and fourth column, respectively. Data are shown for different lattice temperatures T_L and FEL power densities P_{FEL}.

	τ exp (ps)	τ theo (ps)	$\Delta T/T$ (%)	T_e (K)
S1 $T_L = 4$ K $P_{\mathrm{FEL}} = 8$ mW	57	47	2	97
S1 $T_L = 60$ K $P_{\mathrm{FEL}} = 8$ mW	31	39	2	100
S1 $T_L = 4$ K $P_{\mathrm{FEL}} = 750$ mW	25	25	20	390
S2 $T_L = 4$ K $P_{\mathrm{FEL}} = 8$ mW	65	51	5.5	104
S2 $T_L = 90$ K $P_{\mathrm{FEL}} = 8$ mW	24	27	4	115
S2 $T_L = 90$ K $P_{\mathrm{FEL}} = 300$ mW	19	23	15	193

from the numerical simulation, we estimate a fourfold increase of the peak electron temperature ($T_e = 390$ K). High pump power data are also shown in Fig. 2(f), where the differential transmission signal measured in S2 at $T_L = 90$ K with $P_{\mathrm{FEL}} =$ 300 mW, is reported. The initial relaxation time (19 ps) is similar to that obtained at high excitation in S1. The peak electron temperature (193 K) is still relatively high, being twice the value obtained with low power pumping. The large peak values for the differential transmission signal and for the electron temperature obtained in S1 and S2 at high pump powers indicate that, in comparison with the low excitation condition, a much larger fraction of electrons in the $|1\rangle$ SB can now relax in the fundamental subband via phonon emission. This fact explains why the relaxation dynamics become faster, as also predicted by the theoretical differential transmission signals shown in Figs. 2(c) and 2(f). Finally, it is worth noticing that, at low lattice temperature and high excitation conditions, [Fig. 2(c)] the numerical model indicates a slowdown of the relaxation dynamic at larger delay time. This is due to the cooling of the electron gas toward the equilibrium lattice temperature, which suppresses the further emission of optical phonons. However, the slowdown is less clear from an experimental point of view. For clarity, the above-discussed values for the initial relaxation time and for the differential transmission and electron temperature peaks are summarized in Table I.

Once our energy balance model has been validated against pump-probe measurements on well-characterized samples, we shall now use in a predictive way the expression Eq. (2) for the electron-phonon scattering rate with calibrated interaction parameters. Our goal is to evaluate the ISB relaxation times of Ge MQWs as a function of the subband energy separation E_{10} of the lattice and electronic temperature and of $n_{2\mathrm{D}}$. The results will then be compared to those we obtained on GaAs MQW using the Frölich Hamiltonian to describe the electron-phonon interaction.

To this purpose, we calculate the net rate for the $|1\rangle \rightarrow |0\rangle$ transition $\langle W_{10}^{\mathrm{net}}\rangle$, defined as

$$\left\langle W_{10}^{\mathrm{net}}\right\rangle = \langle W_{10}^{+}\rangle + \langle W_{10}^{-}\rangle - \langle W_{01}^{+}\rangle - \langle W_{01}^{-}\rangle, \qquad (4)$$

where contributions from $|1\rangle \rightarrow |0\rangle$ and $|0\rangle \rightarrow |1\rangle$ processes involving either absorption or emission of optical phonons have been considered.

Following Ref. [22], the statistical average is given by

$$\langle W_{\mathrm{if}}^{\mp}\rangle = \frac{\int_{E_i}^{\infty} f(E,T_e,\mu)[1 - f(E \pm \hbar\omega_{\mathrm{eff}},T_e,\mu)]W_{\mathrm{if}}^{\mp}(k_i)dE}{\int_{E_i}^{\infty} f(E,T_e,\mu)dE},$$

where the momentum k_i of the initial electronic state and its energy E are linked by $E = E_i + \frac{\hbar^2 k_i^2}{2m_{||}}$.

The statistical average performed over the electronic distribution, evaluated analytically using the expressions derived in Ref. [22], allows us to include in the calculation the effects due to the occupancy factor of the initial and final states in the two subbands. This is relevant to evaluate the correct relaxation time, especially for subband separation close to or below the optical phonon energy. In fact, in this energy region, relaxation times can be largely overestimated if the empty-subbands approximation is assumed [33], as often reported in literature [15–18].

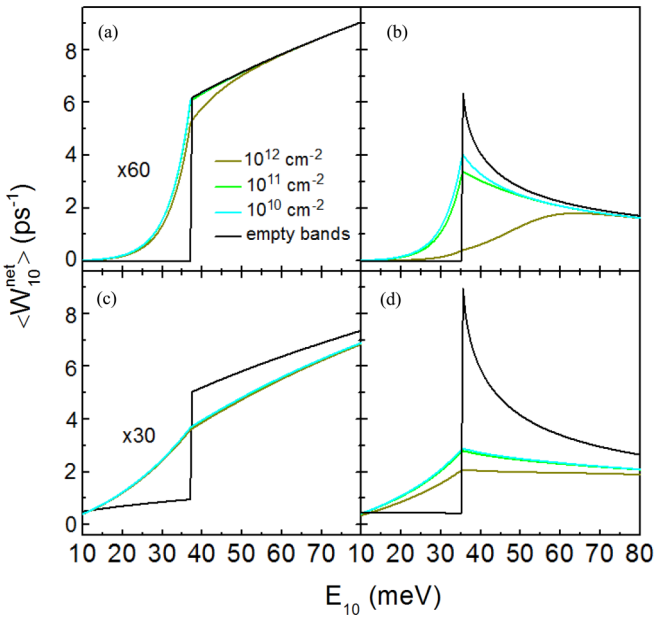

FIG. 3. (Color online) Net scattering rate for the $|1\rangle \rightarrow |0\rangle$ transition, averaged over the Fermi-Dirac distributions with an electron temperature (a), (b) $T_e = 65$ K and (c), (d) $T_e = 350$ K, calculated as function of the subband energy separation E_{10}, for different 2DEG carrier densities. Left and right panels refer to Ge and GaAs QWs, respectively. In the first (latter) case, the electron-phonon scattering is mediated by the deformation potential (polar Frölich) interaction. The phonon occupation follows a Bose-Einstein distribution with temperature (a), (b) $T_L = 15$ K or (c), (d) $T_L = 300$ K. The continuous black line represents the empty band scattering rate as calculated for a single electron at the bottom of the $|1\rangle$ subband. In the left panels, curves have been magnified (a) $\times 60$ and (b) $\times 30$ owing to the much smaller value of the scattering rate in Ge than in GaAs.

The left panels of Fig. 3 show $\langle W_{10}^{\mathrm{net}}\rangle$, calculated as a function of E_{10} at $T_L = 15$ and 300 K and for three values of the 2D electron density $n_{2\mathrm{D}} = 0.1$, 1.0, and 10×10^{11} cm^{-2}, covering the entire range of experimentally available 2DEGs densities. To simulate realistic out-of-equilibrium conditions in real ISB devices, we set $T_e = T_L + 50$ K. For sake of comparison, the $\langle W_{10}^{\mathrm{net}}\rangle$ net rate has been calculated also for GaAs QW, following the same approach outlined in Ref. [11]. The E_{10} subband energy separation has been varied tuning the QW width, and the infinitely deep flat band approximation is assumed for both the Ge and GaAs systems. To better underline the effects due to the electronic population distribution, in Fig. 3, we also plot the empty band $|1\rangle \rightarrow |0\rangle$ transition rate $W_{10} = W_{10}^{+} + W_{10}^{-}$ obtained for a single electron placed at the bottom of the first excited subband (dashed curves). In this latter case and for low lattice temperature (top panels), the empty band transition rate vanishes for E_{10} below the phonon energy due to energy conservation, while at $T_L = 300$ K, it is not zero since $|1\rangle \rightarrow |0\rangle$ transitions with absorption of optical phonons are allowed, providing that the final states have sufficient in-plane momentum. Note also the different functional form of W_{10} for Ge and GaAs: in Ge, the coupling term for the electron-phonon interaction does not depend

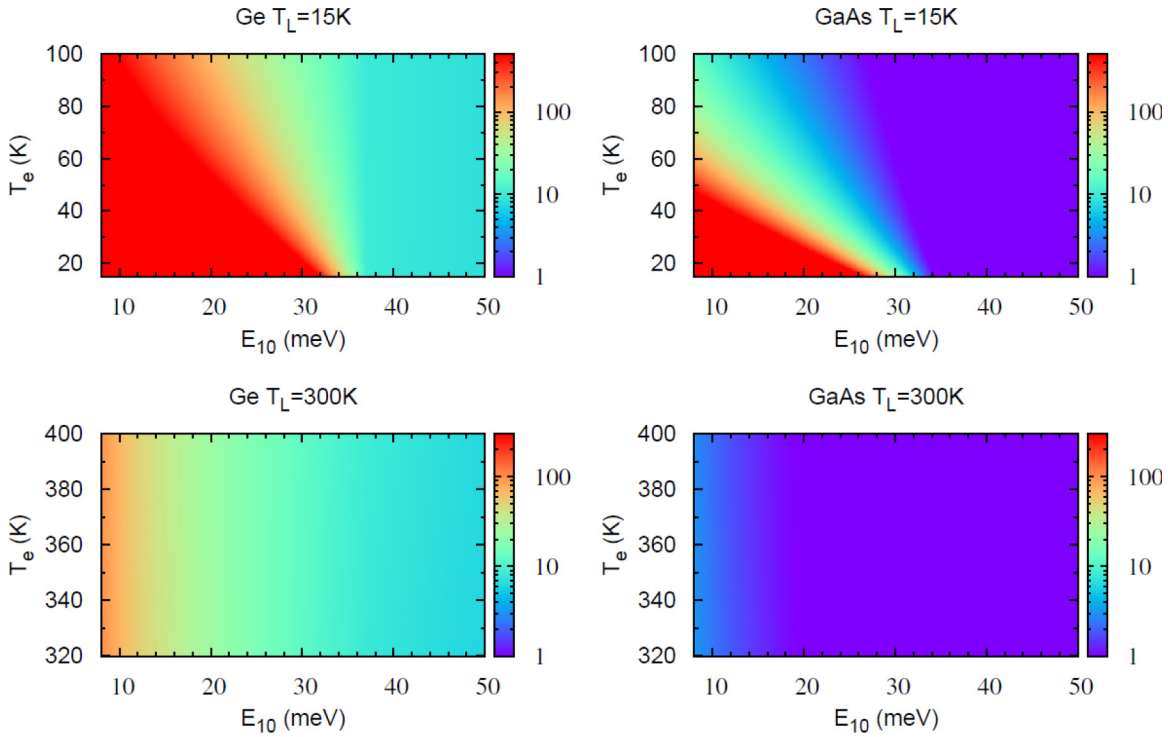

FIG. 4. (Color online) Contour plots of the effective relaxation time $\tau_R = \langle W_{10}^{\rm net}\rangle^{-1}$ measured in picoseconds for Ge (left plots) and GaAs (right plots) QWs, versus E_{10} and T_e, calculated for $n_{2D} = 10^{11}$ cm^{-2}. Note that the logarithmic color scale spans less than three orders of magnitude for better visibility of the most relevant range (1 to 100 ps), while values of τ_R are above 1000 ps (below 1 ps) for low (high) E_{10} and T_e, respectively.

on the exchanged momentum, and then the scattering rate versus the subband energy separation resembles a θ function. On the contrary, in polar materials like GaAs, the coupling term is inversely proportional to the exchanged momentum. It follows that a sharp resonance is present when $E_{10} = \hbar\omega_{\rm LO}$ since, in this case, the initial and final electronic states have the same momentum [note that the optical phonon energy in GaAs is $\hbar\omega_{\rm LO}$(GaAs) = 36.7, very close to the Ge value of $\hbar\omega_{\rm LO}$ (Ge) = 37 meV]. As already pointed out by Lee *et al.* [11] in the GaAs QWs case, the main effect of the electronic distribution is the smearing of the resonance at $E_{10} = \hbar\omega_{\rm LO}$, resulting in a nonvanishing $\langle W_{10}^{\rm net}\rangle$ transition rate also in the energy region below the optical phonon energy. This is a consequence of the presence of thermally excited electrons in the $|1\rangle$ subband whose energy is sufficient to emit optical phonons when relaxing in the fundamental subband. We observe a similar effect in Ge. For instance, defining a relaxation time $\tau_R = \langle W_{10}^{\rm net}\rangle^{-1}$, we find for $E_{10} = 20$ meV a value of $\tau_R \sim 300$ ps at $T_L = 15$ K and $\tau_R \sim 25$ ps at $T_L = 300$ K, respectively. However, the main result emerging from Fig. 3 is that nonradiative transition times in Ge are generally much slower than in GaAs [notice the $\times 60$ ($\times 30$) magnification used in the top (bottom) left panels of Fig. 3]. As an example, the previously reported relaxation times for Ge can be compared with the values of 7 and 0.9 ps found in GaAs for $n_{2D} = 10^{11}$ cm^{-2} at the same temperatures. Finally, it can be concluded that, differently from GaAs, $\langle W_{10}^{\rm net}\rangle$ in Ge is almost independent on the electron density. This is to be attributed to the higher density of states of Ge, due to the four degenerate L conduction valleys. For device applications, this feature can have beneficial consequences in terms of more stable operating conditions.

The dependence of $\tau_R = \langle W_{10}^{\rm net}\rangle^{-1}$ on transition energy and electron temperature is highlighted in the contour plots of Fig. 4, where we set $n_{2D} = 1 \times 10^{11}$ cm^{-2}, a value similar to those found in the studied samples. Results for Ge (left plots) are compared with data calculated for GaAs (right plots) for $T_L = 15$ K (top plots), and $T_L = 300$ K (bottom). Both at low and high (room) lattice temperatures, the two materials display a qualitatively similar behavior. At $T_L = 15$ K, the relaxation time strongly depends on the subband energy separation and rapidly increases when E_{10} becomes smaller than the optical phonon energy. Moreover, a significant dependence on the electronic temperature is found in the $E_{10} < \hbar\omega_{\rm LO}$ region, where $|1\rangle \rightarrow |0\rangle$ transitions with emission of optical phonons can be thermally activated. Due to this mechanism, the relaxation time at fixed E_{10} energy is a decreasing function of T_e. For $T_e > T_L = 300$ K (bottom plots), the dependence on T_e becomes very weak in the whole E_{10} range due to the large fraction of electrons, independently on the transition energy, having sufficient kinetic energy to relax in the $|0\rangle$ subband via optical phonon emission.

We point out that the Ge relaxation times are significantly larger than the GaAs ones in the whole parameter space shown in Fig. 4. In particular, at low T_L and well above the optical phonon energy, we obtain typical Ge relaxation times of $\sim$10 ps, which decreases down to $\sim$6 ps at $T_L = 300$ K. Both these values very favorably compare to the subpicosecond

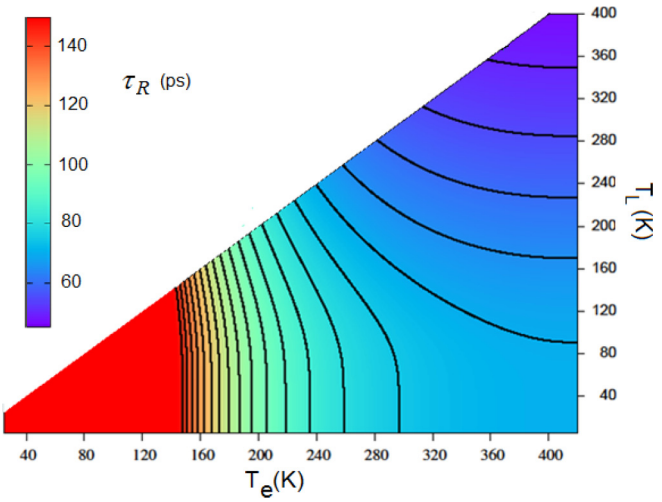

FIG. 5. (Color online) Contour plot of the effective relaxation time $\tau_R = \langle W_{10}^{\rm net}\rangle^{-1}$ in picoseconds for Ge QW versus T_L and T_e with $E_{10} = 12$ meV and $n_{2D} = 10^{11}$ cm^{-2}. The color scale is saturated at 150 ps for clarity, although values of τ_R for low T_L and T_e reach beyond 1000 ps.

relaxation times obtained for GaAs at low and room T_L in the same energy region.

Recently, two quantum cascade laser devices based on Ge QW have been proposed with operating emission energies of 12 and 16 meV [34]. We notice that, for these values of E_{10}, we obtain for Ge at $T_L = 300$ K, $\tau_R = 54$ and 36 ps, respectively, about 30 times the corresponding values for GaAs (1.9 and 1.3 ps, respectively).

We shall now study the relaxation time τ_R as a function of both the lattice and electron temperature. To this aim, we display in the contour plot of Fig. 5 τ_R evaluated at $E_{10} = 12$ meV and $n_{2D} = 1 \times 10^{11}$ cm^{-2} in the portion of the (T_e,T_L) plane where $T_e > T_L$. At this chosen subband separation in the low T_e and T_L parameter region, the relaxation time is larger than 150 ps (the color scale is saturated), while it decreases to about 45 ps when both T_e and T_L are of the order of 400 K. An interesting physical insight comes from the analysis of the isolines orientation shown in the figure. At low lattice temperature, the gradient of τ_R is parallel to the T_e axis. This indicates that the mechanism limiting the relaxation time is the thermal activation, due to an increase in T_e, of an increasing number of energy-allowed $|1\rangle \rightarrow |0\rangle$ transitions with emission of optical phonons. Conversely, the lattice temperature, which controls the phonon population, plays a minor role in this parameter region. The opposite holds at high T_e. In this condition, most of the electrons in the $|1\rangle$ subband have sufficient energy to emit optical phonons, and hence the limiting factor controlling the relaxation time becomes the lattice temperature, as deduced from the orientation of the τ_R gradient, which is now parallel to the T_L axis. In this case, an increase of the lattice temperature increases the number of the phonon-mediated $|1\rangle \rightarrow |0\rangle$ transitions through the $(N + 1)$ phonon population factor. Finally, it is worth noticing that, contrary to that intuitively expected, τ_R does not diverge when $T_e = T_L$. This has to be attributed to the subband dispersion in the $k_\parallel$ plane. In fact, if the QW subbands were dispersionless, as it happens in a genuine two level system, $|1\rangle \rightarrow |0\rangle$ transitions would always correspond to a net positive transfer of energy from the electron gas to the phonon bath. This is not the case for QW 2D systems for which $|1\rangle \rightarrow |0\rangle$ transitions can occur also via phonon absorption, i.e. with a positive net transfer of energy from the phonon bath to the electron gas. Indeed, the quantity that vanishes at $T_e = T_L$, as we have verified, is not the net electronic transition rate $\langle W_{10}^{\rm net}\rangle$ but the net energy transfer rate between the electronic and ionic degrees of freedoms. This latter quantity is proportional to the net (i.e. emission minus absorption) phonon emission rate, which has to be calculated summing over all the initial and final electronic states.

IV. CONCLUSIONS

In summary, we have investigated the nonradiative ISB transitions recombination mechanism in n-type Ge/SiGe MQWs grown on Si, both experimentally and theoretically. For transition energy close to the Ge phonon energy, pump-probe differential transmission measurements have shown very long relaxation times (∼65 ps) at low lattice temperature and pump power. The relaxation time only reduces to ∼20 ps at higher temperature and pump power. We have used an energy balance model to simulate the differential transmission measurements. Calibration of the model on the experimental data has allowed us to extract the physical parameters governing the electron-optical phonon scattering in the Ge/SiGe system, which are a key ingredient for the theoretical design of Ge-based ISB devices. The good agreement of the model predictions with the differential transmission spectra allow us to conclude that a single set for the effective phonon energy $\hbar\omega_{\rm eff} = 37.04$ meV and deformation potential $\Xi_{\rm OP} = 3.5 \times 10^8$ eV/cm well describes the electron-optical phonon coupling in all the investigated conditions.

In the second part of the paper, we have used our model in a predictive way to evaluate the nonradiative ISB $|1\rangle \rightarrow |0\rangle$ scattering rates averaged over the electron distribution, in the lattice and electron temperatures, and in the subband separation energy parameter space. We find that ISB room-temperature $|1\rangle \rightarrow |0\rangle$ relaxation times for the Ge/SiGe systems with subband separation below the phonon energy are generally shorter than that previously calculated by means of an oversimplified empty band approximation. Nevertheless, the relaxation time remains longer than 10 ps, also for transition energies above the Ge optical phonon energy. Furthermore, a systematic comparison with relaxation times evaluated for GaAs-based QW systems shows that, in Ge/SiGe QWs, the relaxation times are generally expected to be one order of magnitude longer. The results presented in this paper support the feasibility of Si-compatible Ge-based ISB photonic devices operating at higher temperature with respect to those based on III-V semiconductors.

ACKNOWLEDGMENTS

One of the authors (M.O.) acknowledges support from Italian Ministry of Research under the program “FIRB Futuro in Ricerca”, Grant No. RBFR08N9L9.

[1] A. Valavanis, L. Lever, C. A. Evans, Z. Ikonić, and R. W. Kelsall, Phys. Rev. B **78**, 035420 (2008).

[2] T. Asano, M. Tamura, S. Yoshizawa, and S. Noda, Appl. Phys. Lett. **77**, 19 (2000).

[3] P. Chaisakul, D. Marris-Morini, G. Isella, D. Chrastina, X. Le Roux, S. Edmond, E. Cassan, J.-R. Coudevylle, and L. Vivien, Appl. Phys. Lett. **98**, 131112 (2011).

[4] O. Fidaner, A. K. Okyay, J. E. Roth, R. K. Schaevitz, Y.-H. Kuo, K. C. Saraswat, J. S. Harris, and D. A. B. Miller, IEEE Phot. Technol. Lett. **19**, 1631 (2007).

[5] J. E. Roth, O. Fidaner, R. K. Schaevitz, Y.-H. Kuo, Th.I. Kamins, J. S. Harris, and D. A. B. Mille, Opt. Express **15**, 5851 (2007).

[6] Y.-H. Kuo, Y. K. Lee, Y. Ge, S. Ren, J. E. Roth, T. I. Kamins, D. A. B. Miller, and J. S. Harris, Nature **437**, 1334 (2005).

[7] A. Samarelli, L. Ferre Llin, S. Cecchi, J. Frigerio, T. Etzelstorfer, E. Müller, Y. Zhang, J. R. Watling, D. Chrastina, G. Isella, J. Stangl, J. P. Hague, J. M. R. Weaver, P. Dobson, and D. J. Paul, J. Appl. Phys. **113**, 233704 (2013).

[8] J. Yin and R. Paiella, Appl. Phys. Lett. **98**, 041103 (2011).

[9] M. Helm, in *Intersubband Transitions in Quantum Wells: Physics and Device Applications*, edited by E. R. Weber, R. K. Willardson, H. C. Liu, and F. Capasso (Academic Press, San Diego, 2000).

[10] H. Rücker, E. Molinari, and P. Lugli, Phys. Rev. B **45**, 6747 (1992).

[11] S.-C. Lee, I. Galbraith, and C. R. Pidgeon, Phys. Rev. B **52**, 1874 (1995).

[12] M. A. Stroscio, *Phonons in Nanostructures* (Cambridge University Press, Cambridge, 2001).

[13] B. K. Ridley, Phys. Rev. B **39**, 5282 (1989).

[14] K. Driscoll and R. Paiella, Appl. Phys. Lett. **89**, 191110 (2006).

[15] G. Sun, H. H. Cheng, J. Menéndez, J. B. Khurgin, and R. A. Soref, Appl. Phys. Lett. **90**, 251105 (2007).

[16] L. Lever, A. Valavanis, Z. Ikonić, and R. W. Kelsall, Appl. Phys. Lett. **92**, 021124 (2008).

[17] D. J. Paul, Laser & Photonics Reviews **4**, 610 (2010).

[18] L. Lever, A. Valavanis, C. A. Evans, Z. Ikonic, and R. W. Kelsall, Appl. Phys. Lett. **95**, 131103 (2009).

[19] M. S. Vitiello, G. Scamarcio, V. Spagnolo, C. Worrall, H. E. Beere, D. A. Ritchie, C. Sirtori, J. Alton, and S. Barbieri, Appl. Phys. Lett. **89**, 131114 (2006).

[20] M. De Seta, G. Capellini, Y. Busby, F. Evangelisti, M. Ortolani, M. Virgilio, G. Grosso, G. Pizzi, A. Nucara, and S. Lupi, Appl. Phys. Lett. **95**, 051918 (2009).

[21] B. N. Murdin, W. Heiss, C. J. G. M. Langerak, S.-C. Lee, I. Galbraith, G. Strasser, E. Gornik, M. Helm, and C. R. Pidgeon, Phys. Rev. B **55**, 5171 (1997).

[22] M. Virgilio, G. Grosso, G. Pizzi, M. De Seta, G. Capellini, and M. Ortolani, Phys. Rev. B **86**, 205317 (2012).

[23] M. De Seta, G. Capellini, M. Ortolani, M. Virgilio, G. Grosso, G. Nicotra, and P. Zaumseil, Nanotechnology **23**, 465708 (2012).

[24] M. Ortolani, D. Stehr, M. Wagner, M. Helm, G. Pizzi, M. Virgilio, G. Grosso, G. Capellini, and M. De Seta, Appl. Phys. Lett. **99**, 201101 (2011).

[25] Y. Busby, M. De Seta, G. Capellini, F. Evangelisti, M. Ortolani, M. Virgilio, G. Grosso, G. Pizzi, P. Calvani, S. Lupi, M. Nardone, G. Nicotra, and C. Spinella, Phys. Rev. B **82**, 205317 (2010).

[26] M. Bonfanti, E. Grilli, M. Guzzi, M. Virgilio, G. Grosso, D. Chrastina, G. Isella, H. Von Känel, and A. Neels, Phys. Rev. B **78**, 041407(R) (2008).

[27] D. Stehr, S. Winnerl, M. Helm, T. Dekorsy, T. Roch, and G. Strasser, Appl. Phys. Lett. **88**, 151108 (2006).

[28] S. Lutgen, R. A. Kaindl, M. Woerner, T. Elsaesser, A. Hase, H. Künzel, M. Gulia, D. Meglio, and P. Lugli, Phys. Rev. Lett. **77**, 3657 (1996).

[29] S. Rudin and T. L. Reinecke, Phys. Rev. B **41**, 7713 (1990).

[30] C. Jacoboni, F. Nava, C. Canali, and G. Ottaviani, Phys. Rev. B **24**, 1014 (1981).

[31] M. V. Fischetti, D. J. DiMaria, S. D. Brorson, T. N. Theis, and J. R. Kirtley, Phys. Rev. B **31**, 8124 (1985).

[32] When the scattering parameters are taken from Ref. [30], a worse agreement with the experimental data is generally obtained.

[33] T. Mueller, W. Parz, G. Strasser, and K. Unterrainer, Phys. Rev. B **70**, 155324 (2004).

[34] A. Valavanis, T. V. Dinh, L. J. M. Lever, Z. Ikonić, and R. W. Kelsall, Phys. Rev. B **83**, 195321 (2011).